Removing Biases in Oceanic Turbulent Kinetic Energy Dissipation Rate Estimated from Microstructure Shear Data⬙

BRUNO FERRON⬤,[a] P. BOURUET AUBERTOT,[b] Y. CUYPERS,[b] AND C. VIC[a]

[a] *University Brest, CNRS, IFREMER, IRD, Laboratoire d'Océanographie Physique et Spatiale, IUEM, Brest, France*
[b] *LOCEAN-IPSL, Sorbonne University (UPMC, Univ Paris 06)-CNRS-IRD-MNHN, Paris, France*

ABSTRACT: To calculate a turbulent kinetic energy dissipation rate from the microstructure vertical shear of the horizontal velocity via a spectral analysis, shear spectra need first to be cleaned from vibrations of the moving vehicle. Unambiguously, this study shows that the spectral cleaning must be applied all over the frequency range and not only at frequencies larger than 10 Hz, as a recent study suggested. For a Vertical Microstructure Profiler (VMP-6000), not correcting for vehicle vibrations below 10 Hz leads to overestimated dissipation rates from 50% to 700% for usual downcast velocities and for weak dissipation rates ($\varepsilon < 1 \times 10^{-9}$ W kg^{-1}). Vibrations concern all vehicles, but the exact vibrational frequency signature depends on the vehicle shape and its downcast velocity. In any case, a spectral cleaning over the whole frequency range is strongly advised. This study also reports on a systematic low bias of inferred dissipation rates induced by the spectral cleaning when too few degrees of freedom are available for the cleaning, which is usually the default of the standard processing. Whatever the dissipation rate level, not correcting for the bias leads to underestimated dissipation rates by a factor 1.4–2.7 (with usual parameters), the exact amplitude of the bias depending on the number of degrees of freedom and on the number of independent accelerometer axes used for the cleaning. It is strongly advised that such a bias be taken into account to recompute dissipation rates of past datasets and for future observations.

KEYWORDS: Turbulence; Mixing; In situ oceanic observations; Data processing/distribution

1. Introduction

Microstructure shear data sampled by airfoil shear probes have been used for decades to measure the dissipation rate of turbulent kinetic energy ε and to diagnose the intensity of oceanic mixing. Such shear probes are mounted on dedicated vehicles [e.g., High Resolution Profiler (HRP; Polzin and Montgomery 1996); Vertical Microstructure Profiler (VMP; rocklandscientific.com/products/profilers); Microstructure Sonde (MSS; www.sea-sun-tech.com/product-category/probes/mss-probes)] and more recently equipped other nondedicated platforms such as gliders and floats. Each of these vehicles has a specific vibrational frequency signature when it moves into seawater that is due to vortex shedding. Vortex-inducedvibrations (VIVs) depend on the shape of the vehicle, on external equipment (additional sensors, beacons, flags, etc.) attached to the vehicle, and on its profiling velocity. Airfoil shear probes sense high-frequency velocity fluctuations larger than 0.06–0.1 Hz (Osborn and Thomas 1973; Lueck 2016) so that any VIV with a signature above 0.1 Hz contaminates the real oceanic shear sampled by the shear probes.

Because the evaluation of a dissipation rate is calculated from microstructure shear spectra on a specific frequency/wavenumber range (usually above 0.5 and below 100 Hz), it is fundamental to know what the distribution and intensity of VIVs in this frequency/

wavenumber range are (Levine and Lueck 1999). VIV spectrum adds to real oceanic shear spectrum to produce an apparent shear spectrum. Using the same notations as Goodman et al. (2006, G06 hereinafter), the measured apparent shear spectrum Φ_m is the sum of the real oceanic shear spectrum for which we are looking (Φ_o) plus the contribution of the platform vibrations measured by the accelerometers:

$$\Phi_m = \Phi_o + \boldsymbol{\beta}_l \boldsymbol{\chi}_l^*, \tag{1}$$

where the transfer function $\boldsymbol{\beta}$ reads

$$\beta_l = \boldsymbol{\chi}_k \Gamma_{kl}^{-1}, \tag{2}$$

with Γ_{kl} being the cross-spectrum matrix component between accelerometers oriented along the axes k and l (with $k, l = 1, 2,$ or 3 denoting the axis number) and with $\boldsymbol{\chi}_l$ being the cross-spectrum matrix component between shear and the accelerometer in the direction l; the asterisk is the complex conjugate, and repeated indices imply a summation (for more details, the reader is referred to G06). In presence of weak noise on shear data and assuming that platform vibrations are uncorrelated with oceanic turbulence, Eq. (1) can be expressed in terms of the magnitude-squared coherence between accelerometers and the measured shear Γ^2 (e.g., Lucas and Otnes 2010), as

$$\Phi_o = (1 - \Gamma^2)\Phi_m. \tag{3}$$

Equation (3) states that the true oceanic spectrum is equal to the measured spectrum minus the coherent spectral part between accelerometers and shear sensors.

Corresponding author: Bruno Ferron, bruno.ferron@ifremer.fr

Ignoring VIV impact on shear data tends to produce overestimated dissipation rates. Note that the frequency/wavenumber range increases with the intensity of oceanic turbulence since the Kolmogorov cutoff wavenumber increases. Thus, dissipation rates estimated in strongly turbulent flows are statistically more reliable than for weakly turbulent flows. Indeed, in weakly turbulent flows, the resolved shear sensor spectral range shrinks and the shear signal-to-noise ratio decreases.

In strongly turbulent flows ($\varepsilon > 1 \times 10^{-7}$ W kg^{-1}), VIVs may be less of a problem since the signal-to-noise ratio is high, the oceanic turbulence shear spectral levels are often significantly above VIV spectral levels. For moderate turbulence, VIVs can be avoided in part by carefully choosing the upper wavenumber limit of validity of the measured shear spectra and using fits to a theoretical shear spectrum (Nasmyth 1970) and/or the presence of a local spectral minimum. In weakly turbulent environments, the valid frequency range is smaller and the fit to Nasmyth spectrum less reliable, the signal-to-noise ratio decreases, and VIVs can significantly increase the estimated level of real oceanic turbulence.

Most of the recent microstructure instruments are equipped with multiaxis accelerometers to sense vehicle vibrations. To get the real oceanic shear spectra Φ_o, VIVs are then classically removed from the measured shear data Φ_m using the spectral coherence between accelerometers and shear sensors following Eq. (1) (G06 processing).

In a recent paper, Thurnherr et al. (2020, T20 hereinafter) suggested that applying the G06 processing to the whole resolved frequency range significantly underestimates oceanic turbulence intensity in weakly turbulent environments. They noticed that dissipation rates coming from two microstructure datasets of the same region were inconsistent by a factor of up to 10. Both datasets come from a repeated transect around the Brazil Basin Fracture Zone valley near 21°S. The first one was collected in 1997 (Polzin et al. 1997; St. Laurent et al. 2001) with the HRP, for which no accelerometer data were used to clean shear data, and the second was collected in 2015 (Clément et al. 2017) with a VMP equipped with accelerometers to clean shear data. T20 identified that G06 correction applied indiscriminately to all frequencies (as has been done classically) was the source of the inconsistency in dissipation rate estimates issued from the VMP when turbulence was weak. T20 further found that applying G06 only to frequencies larger than 10 Hz and leaving lower frequencies uncorrected solved for the inconsistency. After having noticed that some accelerometer spectra looked like the theoretical spectrum of oceanic turbulence, T20 proposed the following explanation: oceanic turbulence transfers its momentum to the vehicle at low frequency/wavenumber. Thus, below 10 Hz, accelerometers mainly record real oceanic turbulence rather than VIVs. Applying G06 processing below 10 Hz then removes real oceanic turbulence from the shear data and produces dissipation rates that are too small by up to a factor of 10. That is why T20 suggested to apply the G06 correction only to frequencies larger than 10 Hz. One could go a step farther in the T20 reasoning and note that, since oceanic turbulence transmits its momentum to the vehicle, then the measured shear is underestimated, and part of the vibrations recorded by the

accelerometers should be added to the measured signal instead of being removed. Note that microstructure processing is not the main focus of T20; despite the implications of their suggestions, their appendix about the sensitivity of dissipation rates to data processing does not provide much detail.

The Taylor (1935) scaling analysis of the turbulent kinetic energy gives the order of magnitude of the turbulent velocities u' such that $u' = c(\varepsilon l)^{1/3}$, where c is a constant close to 1 and l is the length scale of the energy-containing eddies. With a typical instrument downcast velocity of 0.6 m s^{-1} and taking the lowest frequency of the shear spectral range so that l is maximum (i.e., at 0.5 Hz, $l = 1.2$ m), the order of magnitude of u' is 10^{-3} m s^{-1} for $\varepsilon = 10 \times 10^{-10}$ W kg^{-1}. Are such oceanic turbulent velocities able to imprint coherent accelerations at 0.5 Hz on the vehicle? If not, it is tempting to test the alternative hypothesis: not correcting data for VIVs at low frequencies overestimates dissipation rates. In any case, robust arguments based on data analyses are needed.

Since a large fraction of the ocean is far from energetic sources of turbulence and thus remains relatively quiet with low levels of turbulence ($\varepsilon < 5 \times 10^{-10}$ W kg^{-1}), the point raised by T20 is of importance to diagnose the real level of background turbulence and mixing. Because most of (if not all) current microstructure shear data are accompanied by concurrent accelerometer data and corrected using G06, our community needs to clearly identify whether the point raised by T20 is valid or not. Over- or underestimating the background level of turbulence has some implications on the inferred global oceanic circulation and is of importance for the modeling community. It has also a direct impact on studies focusing on mixing efficiency in weak turbulence.

In this paper, we take advantage of several datasets acquired with a VMP-6000 in weakly turbulent environments to explore the sensitivity and robustness of T20 suggestions. These datasets exhibit various levels of VIVs to test T20 hypothesis. Section 2 describes the datasets and the methods used in the study. Section 3 compares the G06 classical approach (correction applied to all frequencies) and T20 approach on profiles having different levels of VIVs to identify possible biases. Section 4 concludes with recommendations for the community.

2. Datasets and methods

The study relies on microstructure shear profiles from three cruises that were sampled by a VMP free falling at different velocities in weak-to-moderate turbulence ($\varepsilon < 10^{-8}$ W kg^{-1}) (Ferron et al. 2021). To change the VMP downcast velocity, the VMP was equipped with two 70-mm-diameter steel weights of different length and with 0, 2, or 4 drag brushes (Table 1). The larger the downcast velocity is, the more intense the VIVs will be. Simultaneous profiles of dissipation rates done at the same place should be independent of the VIV intensity, if properly removed. Since no simultaneous profiles were available, repeated profiles are used in this study, which unfortunately also encompasses some time variability in the observed oceanic turbulence. Thus, a statistical approach

TABLE 1. Selected VMP profiles sampled during the VAD 2013, MEDOCC 2014, and MoMAR 2021 cruises. Column 6 shows the downcast speed w averaged between 100 dbar and the bottom of the profile; w changed as a function of the number of installed drag brushes and weight (column 4). Column 7 shows the depth-averaged dissipation from the G06 and T20 processings (ε_{G06} and ε_{T20}, respectively), and column 8 is their depth-averaged ratio $\langle r_\varepsilon \rangle = \langle \varepsilon_{T20}/\varepsilon_{G06} \rangle$.

Cruise name and year	Profile No.; time/date	Lat, lon; max pressure reached (dbar)	No. of drag brushes; VMP weight length (cm)	Shear channel used for dissipation rate	$\langle w \rangle$ 100–bottom (cm s^{-1})	$\langle \varepsilon_{G06} \rangle$; $\langle \varepsilon_{T20} \rangle$ ($\times 10^{-10}$ W kg^{-1})	$\langle r_\varepsilon \rangle$ ($=\langle \varepsilon_{T20}/\varepsilon_{G06} \rangle$)
VAD 2013	4; 1735 UTC 29 Nov 2013	43°06.04′N, 06°40.69′E; 833	0; 21	1	77	2.9; 8.7	8.9
	6; 1015 UTC 1 Dec 2013	42°55.34′N, 06°00.63′E; 828	2; 21	1	57	9.1; 16	5.4
	7; 1136 UTC 1 Dec 2013	42°55.24′N, 06°00.74′E; 822	4; 21	1	47	9.1; 16	3.7
	9; 1351 UTC 1 Dec 2013	42°55.37′N, 06°00.62′E; 517	4; 17	1	36	4.3; 8.2	2.4
MEDOCC 2014; Tyrrhenian Sea	20; 0925 UTC 3 Apr 2014	39°46.85′N, 11°53.00′E; 2498	0; 16	2	36	0.88; 2.5	4.6
	30; 0030 UTC 8 Apr 2014	39°47.00′N, 11°53.14′E; 3483	0; 18	2	55	0.51; 4.1	16
MEDOCC 2014; Sicily Channel	24–29; 1235–1904 UTC 6 Apr 2014	37°22.78′N, 11°35.63′E; 450	0; 18	2	58	1800; 2400	1.5
MoMAR 2021	4; 1803 UTC 2 Jun 2021	37°17.739′N, 32°16.790′W; 1611	0; 16	2	41	8.3; 16	2.7
	5; 2035 UTC 2 Jun 2021	37°17.554′N, 32°16.846′W; 1598	0; 18	2	60	3.3; 6.8	4.4
	9; 1809 UTC 5 Jun 2021	37°17.726′N, 32°16.809′W; 1636	0; 16	2	32	4.1; 7.2	2.4
	10; 2035 UTC 5 Jun 2021	37°17.697′N, 32°16.834′W; 1653	0; 18	2	67	4.5; 8.9	4.9

is made to learn about the impact of shear data processing. Note that the two shear probes that equipped the VMP remained the same for a given cruise. Of the two VMP shear channels, the channel that exhibited the lowest noise among the profiles of a given cruise was selected to compute the dissipation rate.

Four VMP stations with repeated profiles located along the French continental slope in the Mediterranean Sea were selected from the VAD 2013 cruise (Hamon 2013) (Fig. 1). One profile was sampled in the Stoechades Canyon on 29 November 2013, and three profiles were repeated near the entrance of the Toulon Canyon on 1 December 2013. All profiles reached more than 800 dbar except the last one, which was limited to 517 dbar to save ship time. Those profiles were initially made for testing the robustness of the dissipation rates with regard to the equipment installed on the VMP. They exhibited different depth-mean downcast velocities from 0.36 to 0.77 m s^{-1}.

Two profiles located in the Tyrrheninan Sea were selected from the MEDOCC 2014 cruise. They are of particular interest since they occur in an environment showing very weak turbulent levels, especially at depth. A profile with a slow mean downcast velocity of 0.36 m s^{-1} was first done, initially to better resolve the small-scale structure of the temperature field, and was stopped near 2500 dbar. It was repeated fewer than 5 days later down to 3483 dbar with a mean downcast velocity of 0.55 m s^{-1}. Six short, repeated profiles from the turbulent Sicily Channel ($\sim$500 m depth) were selected from that same cruise to give a reference in a strongly turbulent environment ($\varepsilon > 10^{-7}$ W kg^{-1}).

Last, four profiles located over the Lucky Strike segment of the Mid-Atlantic Ridge were selected and sampled an environment with weak to moderate turbulence during the MoMAR 2021 cruise (Matabos and Sarrazin 2021). They were made to quantify the dependence of shear data and VIVs on the profiler velocity. Two pairs of profiles with different velocities were repeated as close as possible in time down to 1600 dbar. The time interval between two profiles was near 2.5 h, the duration needed to perform the first profile, to recover the instrument, and to reposition the ship for the second deployment with a different downcast velocity.

The microstructure shear data processing followed the steps described in Ferron et al. (2014), who used ODAS v3.0 (ODAS is the processing software for microstructure equipment made by Rockland Scientific; https://rocklandscientific.com/). A few supplementary parameters, statistics, and differences associated with ODAS v4.3, the latest version available for this study, are provided here. For each dataset, the mean inclination of the VMP to the vertical varies among 3.5°, 4.2°, and 4.9° for cruises VAD, MEDOCC, and MoMAR, respectively. Shear data were first despiked. For each dataset, fewer than 0.5% of the shear data were concerned by spikes. Shear data were then high-pass filtered with a Butterworth filter using a cutoff frequency of 0.4 Hz. Shear spectra are integrated in the wavenumber space to get the shear variance from which the dissipation rate is derived. In ODAS v4.3, the upper limit of integration is determined from a fit to the Nasmyth spectral form, which is approximated by a mathematical formulation that fits the Nasmyth spectrum within 1.1%. The reader is referred to Lueck (2013) for further details. Results
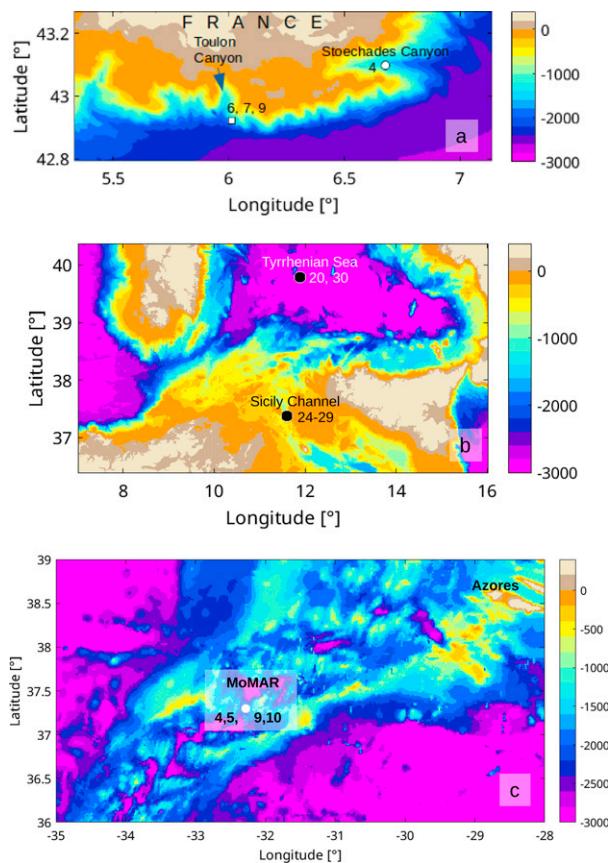
FIG. 1. Selected VMP stations from (a) the VAD 2013 cruise along the French continental slope, (b) the MEDOCC 2014 cruise in the Tyrrhenian and Sicily Channel, and (c) the MoMAR 2021 cruise on the Mid-Atlantic Ridge.

presented in this study do not depend on the small differences in the shear data processing existing among various processing versions; they apply to all ODAS versions up to v4.3. The quality check of the shear data processing (number of spectral components used to estimate the shear variance, mean, and median of the spectral ratio between the observed shear spectra and the fitted Nasmyth spectra, amplitude of the observed shear spectral drop in comparison with the Nasmyth spectral drop, etc.) showed coherent statistics among all the profiles of this study.

Since we deal with weak turbulence, dissipation rates were calculated using 2-s-long Hanning windows with the processing routines ODAS v4.3. All windows were detrended using a parabolic fit before being FFTed (the default processing since ODAS v3.1). Cleaning the shear spectra from vibrations followed the G06 processing included in the ODAS library. Cleaning spectra requires a segment length that is N_{iw} times larger than the length of the FFT window (nFFT). The factor N_{iw} (number of independent windows) must be at least equal to 3 for a VMP-6000 (default value is 4) for the processing to work and to provide sufficient cleaning (the ODAS library returns a warning to the user in case N_{iw} is too small). For the

first part of the study (section 3a), we chose the default value $N_{iw} = 4$; for the second part of the study, N_{iw} was varied from a minimum of 2 (with two-axis accelerometer) or 3 (with three-axis accelerometer) up to a value of 8. For the purpose of this study, the cleaning processing was intentionally modified to follow the T20 processing in such a way that the G06 processing was only applied to frequencies larger than 10 Hz, no correction for vibration contamination being done below 10 Hz. The two processings were then applied to the selected profiles and the results were compared.

3. Results

a. Comparison between G06 and T20 processings

To show the sensitivity of the dissipation rate to the processing, the slowest and fastest profiles from the VAD cruise (Nos. 6 and 9; see Table 1) sampled at the same location and the same day are shown in Fig. 2. The VMP was equipped with drag brushes for those two profiles. Each profile shows a downcast velocity nearly constant as it changes by less than 0.015 m s^{-1} with depth (Fig. 2a). The mean velocity is 0.57 m s^{-1} for profile 6 and 0.36 m s^{-1} for profile 9. For a given processing, dissipation rate profiles 6 and 9 exhibit some common features despite their time difference: enhanced turbulence (10^{-8} W kg^{-1}) above 100 dbar, a minimum around 150 dbar (10^{-10} W kg^{-1}), and another maximum around 200 dbar (10^{-9} W kg^{-1}), followed by weaker dissipation rates down to 490 dbar where a new maximum appears. Profile 9 was stopped at 500 dbar. For a given cast, the T20 processing produces larger dissipation rates than the G06 processing, as expected (Fig. 2b). The difference between the two processings is present at all depths as the ratio of the dissipation rates $r_\varepsilon = \varepsilon_{T20}/\varepsilon_{G06}$ illustrates (Fig. 2c). The slower profile exhibits a depth-averaged dissipation ratio close to 2 with depth variations limited to a small range [1.6 2.4]. The faster profile has a larger depth-averaged ratio of 3.6 with more intense fluctuations in the range [1.5 10]. From 500 to 800 dbar, the faster profile exhibits two different trends in the dissipation ratio that depend on the processing used: the dissipation rate slowly decreases with pressure using G06 processing while it remains nearly constant using the T20 processing.

The examination of the shear spectra as a function of the dissipation rate level shows that the G06 processing decreases the raw shear energy at all frequencies (Fig. 3a, difference between dashed and plain lines). Energetic shear peaks for frequencies equal or larger than 10 Hz are significantly damped with the G06 processing as they are strongly coherent with the peaks recorded by the two horizontal accelerometers a_X and a_Y (Fig. 3b, vertical accelerometer a_z not shown). For lower frequencies (<10 Hz), the shear energy is also decreased by a factor of 2–10 by the G06 processing. At those low frequencies, the acceleration spectral shape looks like the Nasmyth spectral form, consistently with observations that T20 reported. For instance, the Nasmyth spectrum (Fig. 3a, black lines) peaks around 1–2 Hz before it rolls off for dissipation rates around 1–10 $\times$ 10^{-11} W kg^{-1}, which is also

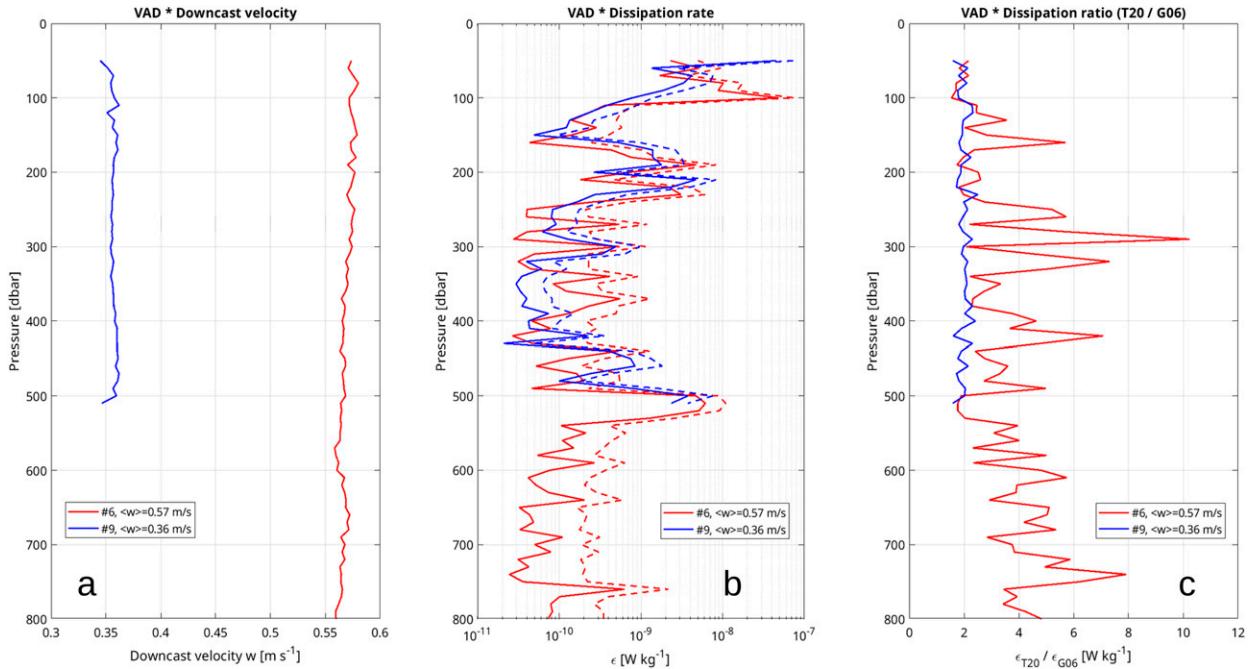FIG. 2. (a) Downcast velocity, (b) dissipation rate ε_{G06} using G06 (solid line) and ε_{T20} T20 (dashed line) processings, and (c) dissipation ratio $\varepsilon_{T20}/\varepsilon_{G06}$ for the faster (No. 6; red) and slower (No 9; blue) profiles sampled at the entrance of the Toulon Canyon on 1 Dec 2013.

observed on the acceleration spectra (Fig. 3b). Those VMP profiles exhibit the same behavior as those examined by T20 in the Brazil Basin. Thus, due to this similarity and following T20, we could also conclude that the accelerometers record oceanic turbulence below 10 Hz and that the G06 spectral correction is inappropriate below 10 Hz. However, a first indication conflicts with this conclusion: if oceanic turbulence was to be recorded by the accelerometers below 10 Hz, the acceleration spectral shape should follow the oceanic (i.e., Nasmyth) spectral shape as turbulence becomes more intense. As turbulent intensity increases, Nasmyth spectrum shows that the energy in the shear shifts toward larger wavenumbers (as Kolmogorov wavenumber increases) but also that the energy at low frequencies increases. Consequently, the level of energy of the accelerometer signal at low frequency should increase with increasing ε as observed for the shear (Fig. 3a). This is not observed, neither for a_X nor for a_Y (Fig. 3b), for which the spectral level of the acceleration remains independent of ε and the peak remains located at the same frequency. We note also that, for this profile, there is a trend to get larger differences between raw and G06 corrected shear spectra with decreasing dissipation rates.

The averaged shear spectra for the common pressure range (50–500 dbar) of the slow and fast profiles do not depend on the downcast velocity at frequencies smaller than 5 Hz (Fig. 4a); for frequencies between 5 and 20 Hz, shear spectra are higher by a factor 2–4 for the fast profile than for the slow profile. Contrastingly, acceleration spectra are directly dependent on the downcast velocity (Fig. 4b) at frequencies smaller than 5 Hz: the peak around 1 Hz of the slow profile increases by a factor of 5 and slightly moves toward

higher frequencies for the faster profile, as VIV theory predicts. At higher frequencies (>5 Hz), the typical level of acceleration does not much depend on the downcast velocity, but peaks associated with VIVs increase in intensity and new peaks appear for both components of acceleration. The difference between raw and G06 corrected shear spectra (Fig. 4a, dashed minus plain lines) does not strongly depend on the downcast velocity. However, this observation may be biased by the time variability between the two casts, and the fact that averaged spectra are dominated by the most energetic individual ones since the difference in spectral amplitude can reach one to several orders of magnitude.

Thus, to better understand the dependence of the spectral corrections of ε below 10 Hz on a wider range of downcast velocities and dissipation rates, we now examine the ratio of the dissipation rates r_ε for all the available casts of the VAD cruise, which cover a wider range of downcast velocities (Table 1 and Fig. 5, top-left panel). A first interesting observation is that r_ε mostly increases below a value $\varepsilon_i \approx 3 \times 10^{-9}$ W kg^{-1}. That is, for $\varepsilon_{G06} > \varepsilon_i$, applying G06 or T20 processing does not have a strong impact on the estimated dissipation rate, though a 40%–60% difference is still observed for the largest dissipation rates of these casts (dots remained above $r_\varepsilon = 1$; Fig. 5, top-left panel). A second interesting observation is that, for a given downcast velocity and for $\varepsilon_{G06} < \varepsilon_i$, there is an increasing difference between the two processings as the dissipation rate decreases. The third important observation is that, for a given ε_{G06} and for $\varepsilon_{G06} < \varepsilon_i$, there is an increasing difference between the two processings as the downcast velocity increases. The largest r_ε (larger than 10) are observed for downcast velocities in
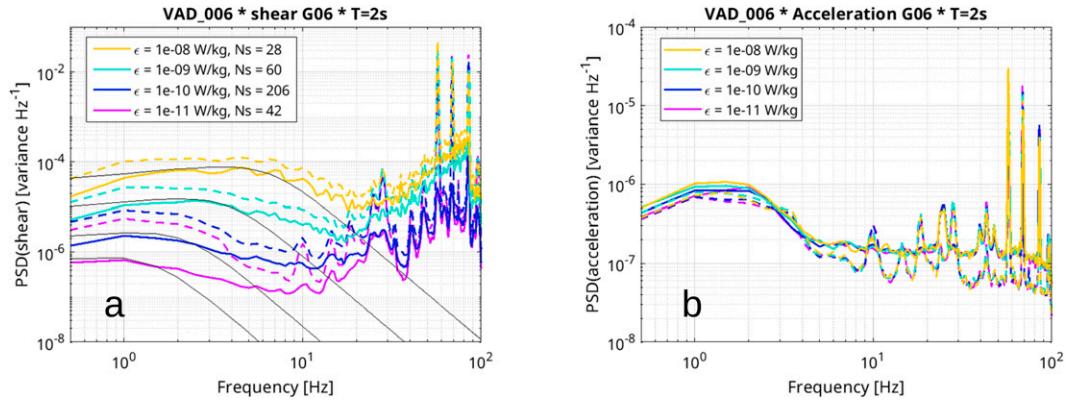
Fig. 3. (a) Raw (dashed lines) and vibration-corrected (solid lines) shear spectra averaged per order of magnitude of ε_{G06} and Nasmyth reference spectra (black lines), (b) a_X (solid lines) and a_Y (dashed lines) acceleration spectra averaged per order of magnitude of ε_{G06}. The fastest profile (No. 6) sampled at the entrance of the Toulon Canyon on 1 Dec 2013 is shown. The number of spectral estimates Ns going into the average is provided in the legend of (a). Here 1e-XX indicates 10^{-XX}.

the range 0.75–0.80 m s^{-1} and for $\varepsilon_{G06} < 5 \times 10^{-11}$ W kg^{-1}. Contrastingly, when the downcast velocity is small (0.35 m s^{-1}), r_ε is not much sensitive to the dissipation rates since it only increases from 1.6 to a maximum of 2.4 as the dissipation rates decreases from 4×10^{-8} to 4×10^{-11} W kg^{-1}.

Those observations conflict with the T20 conclusion that onboard accelerometers mostly record oceanic turbulence below 10 Hz with the VMP, so that raw shear data should not be vibration corrected below 10 Hz. Our observations show that raw shear data below 10 Hz are strongly dependent on the downcast velocity in weakly turbulent regimes, that is, they depend on low-frequency VIVs generated by the VMP motion into seawater. If T20 conclusion was right, we would still observe a strong dependence of r_ε with dissipation rates at a downcast velocity of 0.35 m s^{-1} since the oceanic turbulence remains statistically the same whatever the downcast velocity, and we would not observe a convergence of ε_{G06} and ε_{T20} as the downcast velocity decreases.

To examine if those observations are not specific to the VAD cruise profiles and turbulent environment, we now examine the profiles of the two other cruises, MEDOCC in the Tyrrhenian Sea and MoMAR above the Mid-Atlantic Ridge (Table 1 and Fig. 5, top). For the MEDOCC cruise, dissipation rates are weak and r_ε follows the same behavior as for the VAD cruise, with a large scatter strongly dependent on the downcast velocity for the weakest dissipation rates. The same consistency is found for the moderately turbulent environment above the ridge during the MoMAR cruise. Thus, the observations made for the VAD profiles at a canyon along the shelf break hold for contrasted environments, which is to be expected if low-frequency accelerations are due to VIVs.

b. Identification of a systematic bias associated with the G06 processing

It is now clear that G06 is the processing to use when converting shear data to dissipation rates when vibration sensors
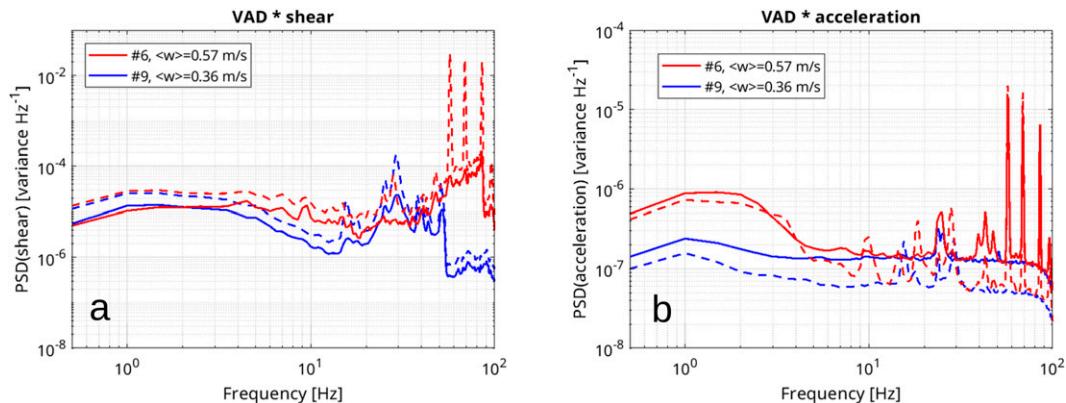

Fig. 4. (a) Raw (dashed lines) and vibration-corrected (solid lines) shear spectra averaged per downcast velocity range and (b) a_X (plain lines) and a_Y (dashed lines) acceleration spectra averaged per downcast velocity range, for the slower (No. 9; blue lines) and faster (No. 6; red lines) profiles sampled at the entrance of the Toulon Canyon and for the pressure range 50–500 dbar; 360 spectral estimates are averaged for each cast.
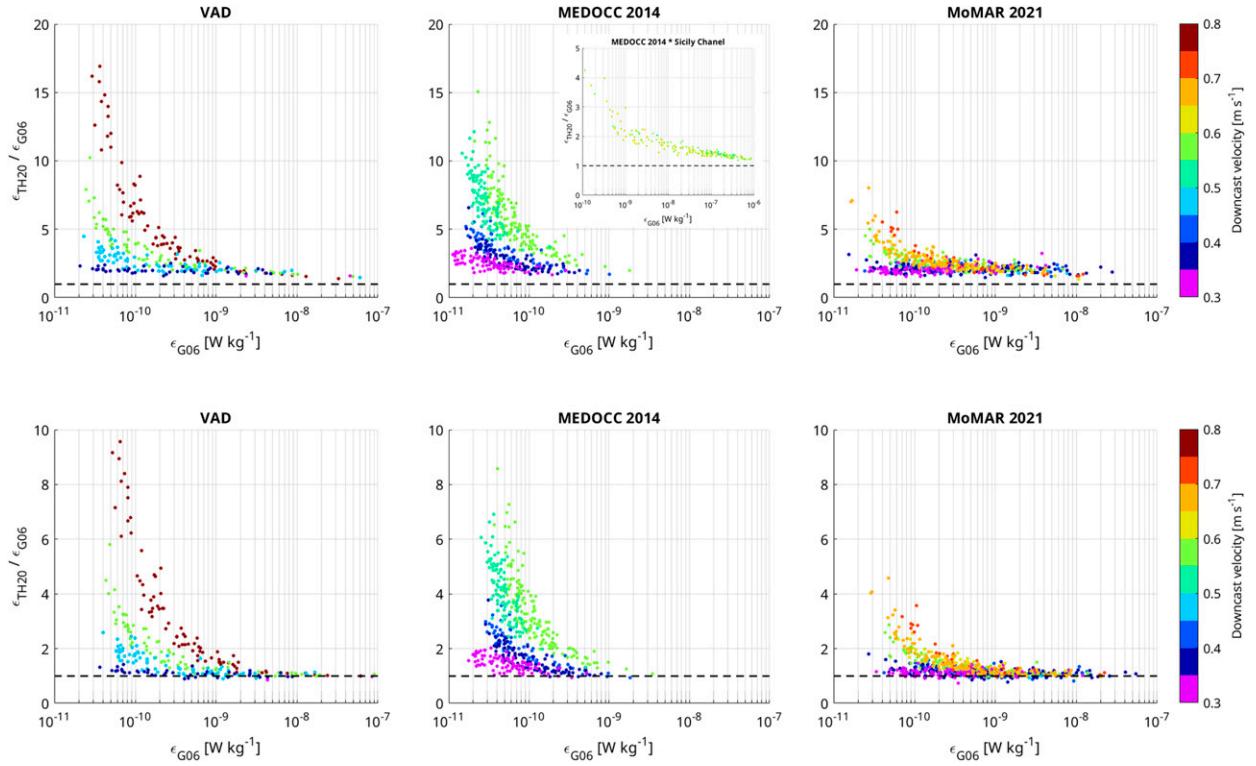
FIG. 5. Scatterplot of the ratio $r_\varepsilon = \varepsilon_{T20}/\varepsilon_{G06}$ as a function of ε_{G06} for the profiles listed in Table 1 and for each cruise. Each dissipation ratio is colored as a function of the downcast velocity (color bar; m s^{-1}). Dashed lines denote $r_\varepsilon = 1$. (top) Standard application of the G06 processing. (bottom) Application of G06 with correction of the systematic factor bias. The top- and bottom-center panels come from data of the Tyrrhenian Sea, and the inset of the top-center panel comes from data of the turbulent Sicily Channel (note that the ordinate of the inset culminates at 5).

equip the microstructure instrument. However, Fig. 5 (top) also points out that, even for the slowest profiles, T20 and G06 do not converge (i.e., $r_\varepsilon = 1$ implies perfect convergence, dashed lines of Fig. 5) for weak to moderate dissipation rates, though the two methods are more consistent for large dissipation rates (Fig. 5, data from Sicily Channel on the inset of top-middle panel of Fig. 5). Indeed, r_ε saturates around 2 for the slowest downcast velocity profiles. It either means that 1) dissipation rates from T20 are still contaminated by weak low-frequency VIVs even at relatively slow profiling velocities or 2) that the G06 processing produces a biased estimate. Despite no profile at a downcast velocity slower than 0.3 m s^{-1} was available for comparison, we can reasonably discard hypothesis 1 by looking at the PSD of the acceleration (a_X, a_Y) for the slowest profile, which is rather flat apart from a weak peak of energy around 1 Hz (Fig. 4b). In the light of those observations and after a careful examination of various versions of the ODAS code (up to v4.3), it turns out that the operator used in G06 produces a "clean" shear spectrum that systematically underestimates the "real" vibration-free shear spectra by a factor, $1/f_b$, whose amplitude depends both on the number of accelerometers (i.e., whether it is 1D, 2D, or 3D axis) and on the number of independent windows N_{iw} used for removing vibrations. This bias in "clean" shear spectra is due to a lack of convergence of the transfer function $\boldsymbol{\beta}$ [Eq. (2)] and

the shear-acceleration cross-spectra $\boldsymbol{\chi}$ [Eqs. (1) and (2)] used in the G06 processing because of the small number of degrees of freedom. Alternatively, Eq. (3) shows that the bias in the "clean" shear spectra is induced by the bias in the estimator of the magnitude squared coherence Γ_e^2. Carter et al. (1973) derived an expression for the mean bias of the estimated Γ_e^2 and showed its dependence on the true value of the coherence Γ_t^2. For two uncorrelated signals, $\Gamma_t^2 = 0$ while Γ_e^2 exhibits the largest mean bias as it varies as $1/N_{iw}$ (the expression was derived for independent windows with no overlap). Consequently, Eq. (3) implies that the ratio of the clean to raw PSD spectra reads $f_b = \Phi_o/\Phi_m = (1 - a/N_{iw})$, with $a = 1$. When the coherence is estimated from a number, N_{acc}, of accelerometers with N_{ow} overlapping windows ($N_{ow} = 2N_{iw} - 1$ for 50% overlapping windows), the statistical model for f_b is slightly modified and reads (R. Lueck 2022, unpublished manuscript)

$$f_b = \Phi_o/\Phi_m = (1 - aN_{acc}/N_{ow}). \tag{4}$$

Integrating the "clean" (but biased) shear spectra produces a systematic underestimated dissipation rate with G06 by a factor $1/f_b$. The bias f_b is independent of the dissipation rate. The convergence of dissipation rates from G06 and T20 for large ε, producing an r_ε close to 1 (Fig. 5, inset of top-middle

TABLE 2. Systematic bias f_b produced by the G06 processing on the shear PSD and on ε as a function of the number of independent sensors recording vibrations (1, 2, or 3—usually the number of axes measured by an accelerometer) and the number of independent windows N_{iw} used for removing vibrations (e.g., if the FFT uses 2-s-long windows and an 8-s-long segment is provided for removing vibrations, then the number of independent windows is 8/2 = 4; for ODAS v4.3, number of independent windows = ql_info.diss_length/ql_info.fft_length). FFT are calculated using an overlap of 50% and each FFTed segment is multiplied by a Hanning (i.e., cosine) window; both are default values of ODAS v4.3. Using other overlap percentages or other windows may change the value of f_b presented in this table. Boldface numbers are the most frequent configurations of microstructure instruments and G06 processing input variables. Numbers in parentheses were estimated with the statistical model (see the main text).

	No. of vibration sensors		
	1	2	3
N_{iw} (=dissipation length/FFT length)			
2	0.66 (0.67)	0.33 (0.33)	Not usable
3	0.80 (0.80)	0.59 (0.60)	0.39 (0.40)
4	0.85 (0.86)	**0.71** (0.71)	**0.56** (0.57)
5	0.89 (0.89)	0.77 (0.78)	0.66 (0.67)
6	0.91 (0.91)	0.81 (0.82)	0.72 (0.73)
7	0.92 (0.92)	0.84 (0.85)	0.76 (0.77)
8	0.93 (0.93)	0.86 (0.87)	0.79 (0.80)

panel; r_ε =1.2 for the Sicily Channel), is explained by the fact that G06 and T20 only differ below 10 Hz and that the frequency band above 10 Hz (where G06 and T20 are equal and thus both equally biased) becomes increasingly dominant as ε increases.

Table 2 provides the values of f_b for several configurations of instruments (equipped with one- to three-axis accelerometer) and for a different number of independent windows set up in the software configuration. The most frequent configurations are highlighted by a bold number: most microstructure instruments are equipped with a 2D-piezzo/MEMS accelerometer or a 3D-axis linear accelerometer and the default number of independent windows is 4 in the ODAS software. In this exercise, f_b was estimated with ODAS v4.3 and makes use of default software parameters for FFT calculations: a Hanning window and a window overlap of 50%; f_b is assessed by looking at the ratio of the clean to raw shear PSD for data that have no spectral coherence between shear and acceleration, that is $\Gamma_t^2 = 0$: in such a case, raw and clean PSD should theoretically be the same (i.e., spectral ratio = 1).

For already processed data, f_b can be assessed by examining the median of the ratios of clean to raw shear PSD at frequencies for which spectral coherence between acceleration and shear is weak. More accurately, f_b can be determined "online" with the user parameters (data segment length, FFT length, overlap, window type) during the processing that estimates the dissipation rate by the following:

1) providing to the G06 processing a time segment of accelerometer and shear data,
2) generating a random rearrangement in time of the accelerometer data (thus, the coherence between shear data and rearranged accelerometer data is expected to be 0),
3) calculating the mean over the whole spectral range of the ratios of clean to raw shear PSD at each frequency (this mean represents one estimate of f_b for a given rearrangement of accelerometer data), and
4) repeating steps 2 and 3 one thousand times and taking the median value of the means calculated at step 3—this

median value is f_b [this step ensures getting a stable value of f_b that does not depend on the variance of f_b as a single estimate (as in step 3) would].

Steps 1 to 4 need only to be done once prior to the usual calculations for determining the clean shear spectra and dissipation rates. Thus, those steps add a negligible amount of CPU time.

In the previously presented examples, the VMP-6000 was equipped with a 3D-axis "linear" accelerometer; a 2-s-long window was prescribed for the FFT with an 8-s-long segment for vibration removal. From Table 2, with N_{iw} = 4 independent windows, we get $1/f_b$ = 1.78, which is consistent with the lowest observed r_ε of Fig. 5 (top) for the slowest downcast velocity. That is, the dissipation rate produced by G06 should be increased by 78% to produce a robust estimate so as to reach the expected unbiased vibration-free dissipation rate. It is important to note that using other window types and/or other FFT window overlap percentages influence the value of f_b since those parameters modify the number of degrees of freedom. For example, switching the Hanning window to a boxcar window (i.e., using no window before FFT) would increase $1/f_b$ from 1.78 to 2.04. Once the bias is corrected, T20 and the modified G06 converge when the downcast velocity is close to 0.3 m s^{-1} (Fig. 5, bottom). Note that the statistical model [Eq. (4)] is able to estimate f_b with an accuracy less than 2% for this set of parameters (Table 2, numbers in parentheses).

As an example to better show the impact of removing the bias on G06 estimates, the dissipation rate was computed with the default G06 processing and with its unbiased version for a number of independent windows, N_{iw} = 2, 3, 4, 8, on profile 6 of the VAD cruise (Fig. 6), which had an averaged downcast velocity of 0.57 m s^{-1}. The unbiased T20 processing is also shown for comparison for N_{iw} = 4. Note that, since the T20 spectrum is the same as the G06 spectrum at frequencies above 10 Hz, the unbiased T20 spectrum is equal to the unbiased G06 spectrum at those frequencies. Below 10 Hz, the unbiased T20 spectrum is unchanged and still equal to the raw spectrum. The default processing (Fig. 6, left panel) clearly
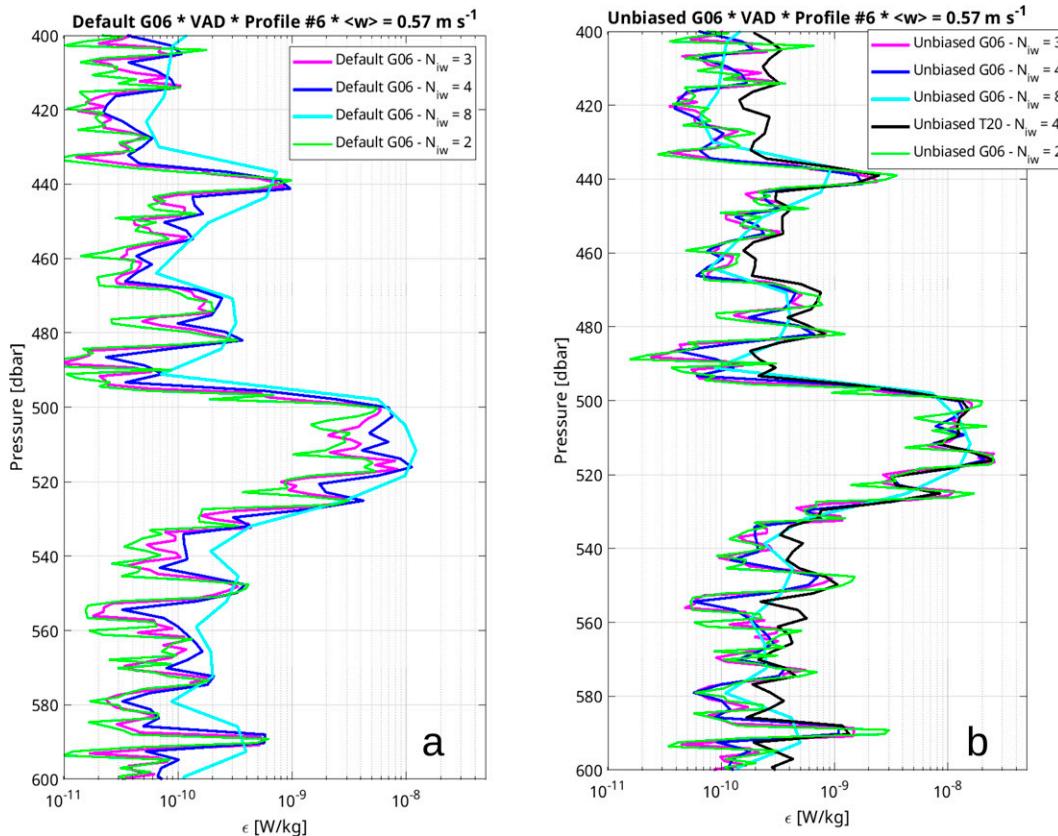
FIG. 6. Comparison of dissipation rates calculated with the default (biased) G06 processing (magenta, blue and cyan lines) for a number of independent windows N_{iw} = 3, 4, and 8 and using the three-axis accelerometer (N_{iw} = segment length used for vibration removal/FFT length = ql_info.diss_length/ql_info.fft_length in ODAS subroutines): (a) default G06 and (b) as in (a), but for unbiased estimates. Unbiased ε_{T20} estimate is provided for comparison with the unbiased ε_{G06} [black and blue lines, respectively, in (b)] for N_{iw} = 4. For N_{iw} = 2 (green line, the most biased estimate; see Table 2), only the two main (i.e., horizontal) accelerometers were provided to the processing.

exhibits the dependence to N_{iw}: the smaller N_{iw}, the weaker the dissipation rate. Note that, increasing N_{iw} has the side effect of increasing the smoothing of the dissipation rate profile as cleaned shear spectra are calculated over overlapping windows of nFFT length and then averaged over the whole segment whose length is N_{iw} × nFFT in the ODAS library. Increasing N_{iw} is done at the expense of losing vertical resolution, which is to be avoided if we need to correlate the dissipation rate profile to other quantities that have a meter-scale resolution (CTD for Thorpe scales, velocity shear from current meters, etc.). Furthermore, even with N_{iw} = 8, dissipation rates are still biased low by almost 25% (Table 2). In contrast, the unbiased spectra give consistent dissipation rate profiles that are independent of N_{iw} apart from the smoothing effect (Fig. 6, right panel), with the advantage of keeping a good vertical resolution for the default N_{iw} (e.g., for N_{iw} = 4 vs 8). When only two accelerometers are provided to the processing, N_{iw} can be reduced to two but the dissipation rate is the most biased (factor 3.5) with the default G06 processing (Table 2; Fig. 6, left panel, green line). In this case, the unbiased dissipation rate estimate also converges toward the

smoother other unbiased estimates that have larger N_{iw} (Fig. 6, right panel), which confirms the robust behavior of the bias removal. On this example, when G06 and T20 are both unbiased, T20 dissipation rate saturates at 2×10^{-10} W kg^{-1} and is unable to see the smaller dissipation rates as it remains contaminated by the low-frequency vibrations of the vehicle (Fig. 6, right panel, blue versus black lines).

4. Discussion

Microstructure shear and accelerometer data show undoubtedly that raw shear spectra need to be corrected from 0.5 to 10 Hz, at least for a VMP-6000. Not removing the vibrations from 0.5 to 10 Hz provides an overestimated dissipation rate for the usual frequency band used for dissipation rate estimation. Having no knowledge at all of the vibrations in the absence of accelerometer prevents any spectral removal of vibrations, with the implication that there is a good chance that weak dissipation rates are biased high. This depends on the frequency distribution and intensity of the vibrations, which are dependent on the downcast velocity and on the shape of

the vehicle (including all added pieces, mast, flags, sensors, etc.). For the VMP-6000 and at a commonly observed downcast velocity in the range 0.5–0.7 m s^{-1}, not accounting for low-frequency vibrations leads to overestimated dissipation rates by 50%–300% for $\varepsilon < 1$–10×10^{-10} W kg^{-1}, and by 200%–700% for $\varepsilon < 0.1$–1×10^{-10} W kg^{-1} (Fig. 5, bottom).

T20 removed the spectral correction of vibrations below 10 Hz since they found that G06 produced dissipation rates that were about a factor of 10 below historical measurements sampled by an HRP two decades before, in a weak turbulent environment. Doing so, they were able to match the HRP historical values. From T20 observations and our study, one can then conclude that HRP dissipation rates are overestimated in weakly turbulent regimes because HRP shear data were not free of vibrations at low frequencies and shear spectra were not corrected using accelerometer data. The amplitude of the HRP overestimation is about 10/f_b, which is less than a factor 10 (10/f_b = 5.7 if T20 used a default 8-s-long segment with their 2-s FFT window). On their sample spectra (their Fig. A1), T20 processing gives an ε of 1.3×10^{-10} W kg^{-1} while G06 gives 0.5×10^{-10} W kg^{-1}. For an 8-s-long segment, the unbiased G06 dissipation rate is $f_b \times 0.5 \times 10^{-10} = 0.9 \times 10^{-10}$ W kg^{-1}; that is, the HRP overestimated the dissipation rate by 50% for this example.

The G06 processing is a correct approach since it removes vibrations all over the usual frequency range (usually frequencies larger than 0.5 Hz). It is the method to be applied to get vibration-free dissipation rate estimates. VIVs are not confined to frequencies above 10 Hz and the energy below 10 Hz recorded by accelerometer data down to 0.5 Hz are not due to oceanic turbulence. For example, the lifting bail of diameter $d = 27$ mm at the top of the VMP, produces a vortex shedding frequency, f_{sh}, between 2 and 6 Hz for a downcast velocity w in the range 0.3–0.8 m s^{-1} [$f_{sh} = 0.2w/d$ for a Reynolds number Re (= wd/ν, where ν is the viscosity of seawater) in the range 6000–16 000].

However, the G06 processing systematically underestimates the dissipation rate by a constant factor that depends both on the number of independent accelerometer axes and on the ratio between the segment length to the FFT length used for removing vibrations. This bias was not reported by G06. However, they noticed that their method produced a broadband correction with a corrected spectrum that was lower by a factor of 2.5 than the uncorrected one. Given their Fig. 2, which shows that the correction impacts all wavenumbers, it is probable that the bias we identified in our study is responsible for a significant part of their observed broadband correction factor. For users of the ODAS library, this bias was not compensated in the library routines up to version v4.3. A new version that takes into account this bias is about to be released (R. Lueck 2022, personal communication) and we invite ODAS users to update their library. For the version 4.3 used in this study, a modified subroutine "get_diss_odas.m" that estimates the bias, corrects the cleaned shear spectra, and provides an unbiased dissipation rate is available in the online supplemental material as a test. This modified subroutine returns a new parameter "diss.f_b" whose value is the bias factor that is estimated from the parameters

the user provides to the subroutine. It is important that all users of the G06 processing (and not only ODAS users) compensate for this systematic bias in the dissipation rate estimates. Whatever the intensity of turbulence, not compensating for this bias produces inconsistent dissipation rate estimates between users and/or cruises and contributes to produce a scatter in the worldwide published dissipation rates and all other linked quantities (mixing rates, turbulent fluxes and their divergence, mixing efficiency, etc.) derived by our community.

Data availability statement. Raw microstructure profiles used in this study are publicly available for noncommercial purpose at the SEANOE data archive (doi.org/10.17882/87306).

REFERENCES

Carter, G. C., C. H. Knapp, and A. H. Nuttall, 1973: Estimation of the magnitude-squared coherence function via overlapped fast Fourier transform processing. *IEEE Trans. Audio Electroacoust.*, **21**, 337–344, https://doi.org/10.1109/TAU.1973.1162496.

Clément, L., A. M. Thurnherr, and L. C. St. Laurent, 2017: Turbulent mixing in a deep fracture zone on the Mid-Atlantic Ridge. *J. Phys. Oceanogr.*, **47**, 1873–1896, https://doi.org/10.1175/JPO-D-16-0264.1.

Ferron, B., F. Kokoszka, H. Mercier, and P. Lherminier, 2014: Dissipation rate estimates from microstructure and finescale internal wave observations along the A25 Greenland–Portugal OVIDE line. *J. Atmos. Oceanic Technol.*, **31**, 2530–2543, https://doi.org/10.1175/JTECH-D-14-00036.1.

——, P. Bouruet-Aubertot, Y. Cuypers, and C. Vic, 2021: Improving microstructure shear data processing in ocean turbulence. SEANOE, accessed 13 June 2021, https://doi.org/10.17882/87306.

Goodman, L., E. Levine, and R. Lueck, 2006: On measuring the terms of the turbulent kinetic energy budget from an AUV. *J. Atmos. Oceanic Technol.*, **23**, 977–990, https://doi.org/10.1175/JTECH1889.1.

Hamon, M., 2013: VAD cruise, RV *L'Europe*. French Oceanographic Cruises, https://doi.org/10.17600/13060130.

Levine, E. R., and R. G. Lueck, 1999: Turbulence measurements from an autonomous underwater vehicle. *J. Atmos. Oceanic Technol.*, **16**, 1533–1544, https://doi.org/10.1175/1520-0426(1999)016<1533:TMFAAU>2.0.CO;2.

Lucas, C. E., and R. Otnes, 2010: Noise removal using multichannel coherence. DRDC Atlantic Tech. Memo. TM 2010-302, 32 pp., https://apps.dtic.mil/sti/pdfs/ADA555503.pdf.

Lueck, R., 2013: Calculating the rate of dissipation of turbulent kinetic energy. RSI Tech. Note 028, 19 pp., https://rocklandscientific.com/support/technical-notes/.

——, 2016: Converting shear-probe, thermistor and microconductivity signals into physical units. RSI Tech. Note 005, 28 pp., https://rocklandscientific.com/wp-content/uploads/2021/12/TN_005.pdf.

Matabos, M., and J. Sarrazin, 2021: MOMARSAT2021 cruise, RV *L'Atalante*. French Oceanographic Cruises, https://doi.org/10.17600/18001296.

Nasmyth, P. W., 1970: Oceanic turbulence. Ph.D. dissertation, University of British Columbia, 109 pp.

Osborn, T., and S. Thomas, 1973: Oceanic shear measurements using the airfoil probe. *Third Biennial Symp. on Turbulence in Liquids*, Rolla, MO, University of Missouri–Rolla, 41–55, https://scholarsmine.mst.edu/sotil/101.

Polzin, K. L., and E. T. Montgomery, 1996: Microstructure profiling with the High Resolution Profiler. *Proc. Microstructure Sensor Workshop*, Mount Hood, OR, Office of Naval Research, 109–115.

——, J. M. Toole, J. R. Ledwell, and R. W. Schmitt, 1997: Spatial variability of turbulent mixing in the abyssal ocean. *Science*, **276**, 93–96, https://doi.org/10.1126/science.276.5309.93.

St. Laurent, L. C., J. M. Toole, and R. W. Schmitt, 2001: Buoyancy forcing by turbulence above rough topography in the abyssal Brazil Basin. *J. Phys. Oceanogr.*, **31**, 3476–3495, https://doi.org/10.1175/1520-0485(2001)031<3476:BFBTAR>2.0.CO;2.

Taylor, G., 1935: Statistical theory of turbulence. *Proc. Roy. Soc. London*, **151**, 421–444, https://doi.org/10.1098/rspa.1935.0158.

Thurnherr, A. M., L. Clement, L. St. Laurent, R. Ferrari, and T. Ijichi, 2020: Transformation and upwelling of bottom water in fracture zone valleys. *J. Phys. Oceanogr.*, **50**, 715–726, https://doi.org/10.1175/JPO-D-19-0021.1.